https://doi.org/10.15407/ujpe71.5.455

D.V. KHOMENKOV, L.YU. MELNICHUK, O.V. MELNICHUK

Mykola Gogol State University of Nizhyn
(2, Grafs'ka Str., Nizhyn 16600, Ukraine; e-mail: khomenkov.dv@ndu.edu.ua)

PECULIARITIES OF THE INFRARED REFLECTANCE SPECTRA OF ZrO_2-BASED MATERIALS WITH DIFFERENT CRYSTALLINE STRUCTURES

The application of infrared reflectance (IRR) spectroscopy to identify crystalline phases in ZrO_2-based materials has been demonstrated. Experimental spectra of powders and ceramics with different structures are presented, and theoretical models are proposed for approximating the IRR spectra on the basis of the frequency dependence of the dielectric permittivity described by the Helmholtz–Kettler formula. Calculations were performed using the Kramers–Kronig relations. Models with one, five, and seven oscillators were used to describe the cubic, tetragonal, and monoclinic ZrO_2 phases, respectively. Simulations were performed while taking the phonon damping coefficients into account. The results obtained showed a pronounced reflectance minimum in the high-frequency spectral interval. Its spectral position corresponds to the high-frequency edge of the "residual-ray band", which is specific to different phases. This minimum appears in the interval of 710–720 cm^{-1} for cubic ZrO_2, 790–800 cm^{-1} for tetragonal ZrO_2, and 820–840 cm^{-1} for monoclinic ZrO_2. It was shown that phonon damping coefficients affect the shape of the IRR spectrum, but have only a minor effect on the spectral position of the high-frequency minimum. This circumstance, together with an analysis of the spectral shape, can serve as a reliable spectral marker for the identification of crystalline phases. Fitting the experimental spectra made it possible to evaluate the static and high-frequency dielectric constants, the frequencies of transverse and longitudinal optical phonons, and the corresponding damping coefficients for ZrO_2-based powders and ceramics with various crystal structures.

Keywords: ZrO_2, crystal structure, vibrational spectra, infrared reflectance spectroscopy, simulation.

1. Introduction

ZrO_2-based materials demonstrate significant practical potential due to their high thermal and chemical stability, wide band gap, and ionic conductivity [1–10]. These materials are widely used in microelectronics, dosimetry, solid-state fuel cells, catalysis, oxygen sensors, and biomedical technologies. A crucial factor affecting the functional properties of ZrO_2 is its crystalline phase structure. The mechanical, optical, and conductive characteristics of ZrO_2 substantially depend on its polymorphic form: monoclinic (m), tetragonal (t), or cubic (c) [1, 2].

Undoped ZrO_2, which is stable in the monoclinic phase at room temperature, transforms into the tetragonal phase when being heated above about 1100 °C, and then into the cubic one if the tempera-

Citation: Khomenkov D.V., Melnichuk L.Yu., Melnichuk O.V. Peculiarities in the infrared reflectance spectra of ZrO_2-based materials with different crystalline structures. *Ukr. J. Phys.* **71**, No. 5, 455 (2026). https://doi.org/10.15407/ujpe71.5.455.

ture grows further [1]. In nanoscale systems (in particular, in powders with a grain size of < 15 nm or in ultrathin films with a thickness of <10 nm), the stabilization of the t- or c-phase can occur even at room temperature [3, 4] due to a substantial surface tension associated with a developed specific surface and a significant ratio between the surface area and the volume of the material. However, during thermal treatment (at about 600–700 °C), grain growth and pronounced crystallization usually lead to a reversion to the monoclinic phase [1, 5].

To stabilize the tetragonal and cubic phases in ZrO_2 powders with larger grain sizes, doping with subvalent cations (e.g., Y^{3+}[6, 7], Ca^{2+} [8], Sc^{3+} [9], or various rare earth elements [7, 10, 11]) is usually applied. The introduction of such impurities creates oxygen vacancies, which compensate for the mismatch between the impurity and zirconium-ion valences and contribute to the stabilization of the t- or c-phases at lower temperatures. Yttrium is one of the most common stabilizers [6, 12] because it remains chemically stable in the cationic sublattice during high-temperature annealing. Along with this, simultaneous doping with several impurities – in particular, scandium and cerium [2], niobium and erbium [13], yttrium and copper [1, 14], and others – is carried out. The choice of the impurity type depends not only on its ability to effectively stabilize the matrix structure, but also on the specific application of doped ZrO_2. At the same time, the structural stability of the crystal lattice under operating conditions is also required in order to avoid degradation of materials and devices based on them. Therefore, monitoring structural transformation is an important task.

Standard methods, such as transmission electron microscopy or X-ray diffraction, provide detailed information about the structural characteristics of materials and structures [1, 15], and they remain indispensable tools. However, unlike X-ray diffraction, the application of electron microscopy requires significant time and effort for specimen preparation, especially when analyzing a large number of samples or when tracking structural changes during their processing.

In this context, the use of optical methods, in particular, Raman scattering (RS) and infrared (IR) spectroscopy, becomes extremely useful. The difference between the methods is that in Raman spectroscopy, the active modes correspond to changes in the molecular polarizability rather than in the dipole moment [16]. This circumstance makes it possible to study modes that are weakly expressed in IR spectra, which makes these methods complementary to each other.

Both methods can be used not only to determine the crystal structure of ZrO_2-based materials, but also to monitor phase transformations. If there are several phases in nanopowders or ceramics, then phonons in different phases can overlap significantly, which leads to a broadening of phonon bands and a shift in their frequencies. This is especially critical for nanostructured materials with mixed phases. In particular, in Ref. [16], the measurements of Raman spectra made it possible to clearly distinguish various polymorphic ZrO_2 phases. Characteristic lines were revealed for the monoclinic phase (at about 177, 188, 472, and 612 cm^{-1}) and the tetragonal phase (at about 145, 266, 472, and 646 cm^{-1}). The amplitude of the peak at 472 cm^{-1} was larger than the maximum at 612 cm^{-1} in the monoclinic phase, but was substantially lower than the intensity of the indicated bands in the tetragonal phase. This fact allowed the contribution made by the monoclinic phase to be clearly distinguished.

The determination of phonon modes in polycrystalline ceramics and nanopowders with small grain sizes can also be hindered by Rayleigh scattering, which can dominate the Raman spectra [15]. In this case, diffuse IRR spectroscopy and the disturbed total internal reflection spectroscopy can be useful because of their suitability for the characterization of fine-grained powders, as well as materials containing grains with various crystal structures.

The presence of a small amount of m- and t-phases of ZrO_2 can be detected in partially destabilized cubic ZrO_2 from their characteristic lines in the IRR spectra [17]. At the same time, these spectra for the cubic and tetragonal phases of nanopowders are slightly different [18], but the characteristic frequencies of the monoclinic phase can be easily detected even at low concentrations [19]. In particular, the presence of a phonon with a frequency of 740–750 cm^{-1} is evidence of the monoclinic phase formation [20]. However, despite a considerable amount of experimental data, IR absorption spectra have been studied mainly for ZrO_2 films [21, 22], which were used as a sub-gate insulator. At the same time, data on IRR spectra of powders or ceramics are rare [15, 20, 23], and theoretical models for IRR spectra of various ZrO_2 phases are de-

scribed only in a few works [19,20,24]. As a result, the quantitative interpretation of IR spectra in materials containing mixed phases or significant concentrations of defects becomes substantially complicated.

In our previous studies [15], we showed that the correlation of the results obtained using electron microscopy and X-ray diffraction methods with optical spectra can provide rapid, non-destructive diagnostics of the phase composition and the structural evolution of ZrO_2-based systems. In this work, we propose theoretical models to describe the IRR spectra of various crystalline phases of ZrO_2 and use them to quantitatively approximate the experimental reflectance spectra of powders and ceramics. At the same time, Raman spectra are applied to confirm the phase composition of the specimens and establish a relation between their optical and structural features.

2. Experimental Part

ZrO_2-based ceramic specimens were prepared using high-purity commercial powders (99.99%). The latter were purchased from Alfa Aesar (Thermo Fisher Scientific, USA; pure ZrO_2), Tosoh (Japan; yttrium-stabilized powder, 8YSZ), and DKKK (Japan; scandium-cerium-stabilized powder, 10Sc1CeSZ) and used without further purification.

To prepare the ceramics, the commercial powders were pressed under a pressure of 50 MPa into pellets 0.5 inch in diameter and annealed at 1400 °C for 3 h in air. A Nabertherm LHT/17 furnace was used to sinter the ceramics. The tablets, together with the oven, were heated to the operating temperature at a rate of 38 °C/min, held at the annealing temperature for 3 h, and then cooled down together with the oven to room temperature.

Besides commercial powders, we also researched powders prepared in the laboratory by means of the coprecipitation method and using high-purity precursors: $ZrO(NO_3)_2 \cdot 6H_2O$ and $Y(NO_3)_3 \cdot 6H_2O$ obtained from Thermo Fisher Scientific (USA). The amount of precursors was chosen to reach the Y_2O_3 content of 3 or 8 mol.% in the final powder. More detailed information on the powder preparation is given in Ref. [15].

Raman spectra were measured in the backscattering geometry using a 785-nm Raman Spectrometer System (StellarNet Inc., USA). The system included a Ramulaser^{TM} 785-nm laser (a wavelength of 785 nm and a half-width of 0.2 nm) with adjustable power (from 0 to 499 mW), a thermoelectrically cooled Raman-HR-TEC-785 spectrometer with a resolution of 4 cm^{-1}, and a high-sensitive CCD detector in the spectral range of 200–2750 cm^{-1}, and a Raman-probe-785 probe, which provided a laser beam 0.15 mm in diameter on the surface of the specimen fixed in the Raman probe holder. The laser power at the specimen surface was kept low to avoid changes in the specimen properties due to heating. Raman spectra were registered with an integration time of 15 s (3 s per spectrum with five-fold averaging). The polarization of scattered light was not analyzed.

Diffuse IRR spectra were registered in a spectral interval of 300–4000 cm^{-1} using a Fourier spectrometer IRTracer-100 equipped with a DRS-8000A diffuse reflectance module (Shimadzu Company, Japan), at an incident angle of excitation light of 10°. A gold mirror was used as a reference. The spectra were registered with a 1-cm^{-1} resolution. To reduce the roughness of the ceramic surface, it was mechanically polished. To analyze the powders using IR spectroscopy, they were mixed with KBr powder (purity 99.99%) in an equal mass ratio and pressed under a pressure of 50 MPa into tablets with a 0.5 inches in diameter.

3. Results and Discussion

3.1. Experimental Raman and IRR spectra of ZrO_2-based specimens with different structures

In Fig. 1, typical Raman spectra are shown for powders (Fig. 1, *a*) and ceramics (Fig. 1, *b*) with a monoclinic (curves *1*), a tetragonal (curves *2*), and a cubic (curves *3*) structure. The specimens with the tetragonal structure were yttrium-doped powders containing 3 mol.% of Y_2O_3 (3YSZ), as well as ceramics based on them and sintered at a temperature of 1400 °C. Powders with 8 mol.% of Y_2O_3 (8YSZ) and ceramics based on it were used as specimens with a cubic structure. It is worth noting that the Raman spectra of zirconium oxide doped with 10 mol.% of Sc_2O_3 and 1 mol.% of CeO_2, (10Sc1CeSZ), which also has a cubic structure, are similar to the spectra of 8YSZ specimens, which are shown by curves *3* in Figs. 1, *a* and 1, *b*.

An analysis of these spectra makes it possible to determine the phonon frequencies characteristic of each phase and the phonon contribution to the Ra-

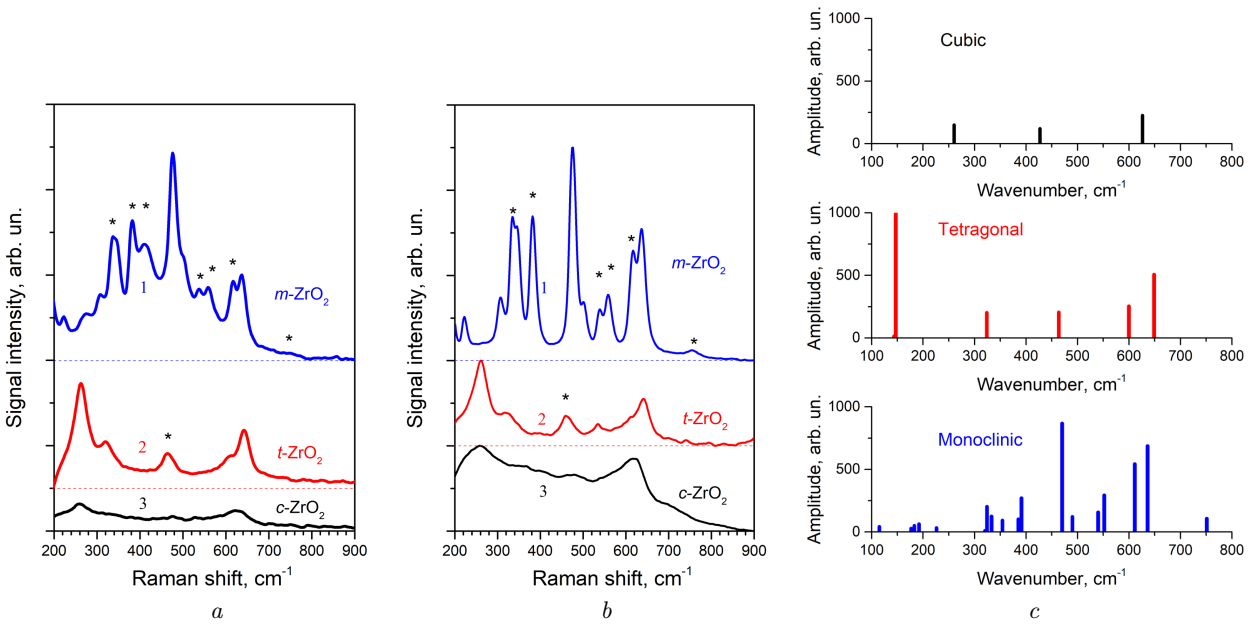

Fig. 1. Raman spectra of ZrO_2 powders (*a*) and ZrO_2 ceramics (*b*): undoped (a monoclinic structure) (*1*), doped with yttrium with a content of 3 mol.% Y_2O_3 (a tetragonal structure) (*2*), and doped with yttrium with a content of 8 mol.% Y_2O_3 (a cubic structure) (*3*). Asterisks mark active IR modes observed in IRR spectra according to Ref. [17, 24]. For clarity, the spectra are shifted along the vertical axis. Corresponding phonon modes determined for various phases (*c*)

man spectrum (Fig. 1, *c*). It can be seen that the phonon modes in the tetragonal and cubic phases are broader and have a smaller amplitude than the modes in the monoclinic phase. At the same time, in the interval 200–800 cm^{-1}, the largest amplitude is observed for phonons at the frequencies $\nu =$ $= 476$ cm^{-1} for m-ZrO_2, $\nu = 260$ cm^{-1} for t-ZrO_2, and $\nu = 642$ cm^{-1} for c-ZrO_2. For the tetragonal phase, these bands are doubled, which is consistent with the data of other authors [12]. The ceramic specimens have more pronounced bands characteristic of each phase (Fig. 1, *b*), especially for monoclinic ceramics (Fig. 1, *b*, curve *1*). This is a result of the grain sintering during the annealing of the ceramics.

In Fig. 2, typical IRR spectra of nanopowders with different crystal structures (Fig. 2, *a*) and ceramics based on them (Fig. 2, *b*) are shown; the corresponding Raman spectra can be seen in Fig. 1, *a* and 1, *b*, respectively. The spectra of the specimens with the monoclinic and tetragonal structures have the largest number of features. Several maxima are observed at about 450, 500, 580, 670, and 760 cm^{-1} for the monoclinic phase; for the tetragonal phase, they are less pronounced (Fig. 2). The IRR spectrum of the cubic phase is broad and structureless.

It is worth noting that the IRR amplitude is the largest for cubic-phase specimens and the smallest for the monoclinic phase. For the Raman signals obtained from those phases, the opposite trend is observed: the maximum amplitude is characteristic of the monoclinic phase, which is especially noticeable for ceramic specimens.

3.2. Theoretical modeling of IRR spectra

To theoretically construct IRR spectra for powders and ceramics with mixed phases, first, it is necessary to consider the case of a single phase (cubic, tetragonal, or monoclinic) and apply the spectral dispersion analysis to determine the phonon modes of each phase. Then, it is possible to analyze materials with mixed phases, revealing the contribution of each specific phase and identifying the corresponding phonon frequencies and damping coefficients. In addition, it is possible to determine whether there are spectral intervals where the conditions for observing polaritons can be fulfilled. This aspect is important in view of the possible creation of optical waveguides based on zirconium oxide.

The IRR spectra were analyzed in the "residual-ray" region of ZrO_2-based materials using the dielec-

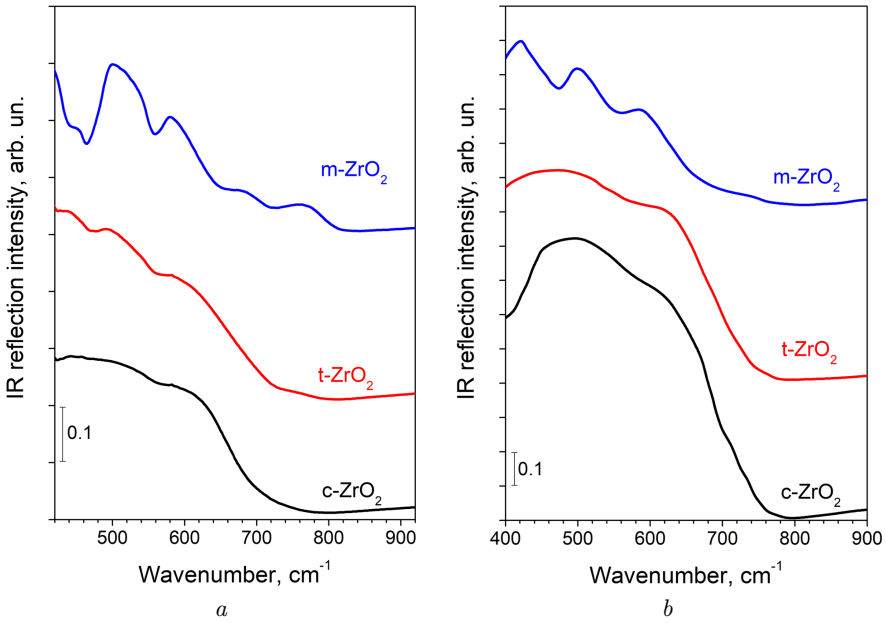

Fig. 2. IRR spectra of (*a*) ZrO_2 nanopowders and (*b*) ZrO_2 ceramics on their basis: undoped (monoclinic structure) (*1*), yttrium-doped with a content of 3 mol.% Y_2O_3 (tetragonal structure) (*2*), and yttrium-doped with a content of 8 mol.% Y_2O_3 (a cubic structure) (*3*). For clarity, the spectra are shifted along the vertical axis

tric permittivity model with the additive and factorized contribution of active optical phonons in the IR interval [25]. The analysis took into account the interaction of infrared radiation only with the phonon subsystem because zirconium oxide is an insulator.

For a single-phase material, the IRR spectrum was modeled on the basis of the frequency dependence of the dielectric permittivity given by the well-known Helmholtz–Kettler formula [26, 27]

$$\varepsilon(\nu) = \varepsilon_1 + i\varepsilon_2 = \varepsilon_\infty + \varepsilon_f, \tag{1}$$

$$\varepsilon(\nu) = \varepsilon_\infty \prod\nolimits_j \frac{\nu_{Lj}^2 - \nu^2 + i\nu\gamma_{Lj}}{\nu_{Tj}^2 - \nu^2 + i\nu\gamma_{Tj}}, \tag{2}$$

where ε_∞ is the high-frequency dielectric constant; ε_f is the contribution of active transverse optical (TO) and longitudinal optical (LO) phonons with the frequencies ν_T and ν_L, respectively; γ_f is the corresponding phonon damping coefficient; and ν is the IR radiation frequency. The real, $\varepsilon_1(\nu)$, and imaginary, $\varepsilon_2(\nu)$, parts of the dielectric permittivity can be obtained by solving the inverse problem of IRR spectroscopy. The reflectance is calculated using the formula

$$R\,(\nu) = \left[\frac{\sqrt{\varepsilon\,(\nu)} - 1}{\sqrt{\varepsilon\,(\nu)} + 1}\right]^2. \tag{3}$$

To simplify the calculations, Eq. (3), using Eq. (2) for the dielectric permittivity, was transformed into the form

$$R(\nu) = \frac{\sqrt{K}_0 - \sqrt{2\left(\sqrt{K}_0 + \varepsilon_1\right)} + 1}{\sqrt{K}_0 + \sqrt{2\left(\sqrt{K}_0 + \varepsilon_1\right)} + 1}, \tag{4}$$

where $K_0 = \varepsilon_1^2 + \varepsilon_2^2$, $A = \varepsilon_\infty$, $B = \varepsilon_0 - \varepsilon_\infty$,

$$y_1 = \left(\frac{\nu}{\nu_T}\right)^2, \quad D = \left(\frac{\gamma_f}{\nu_T}\right)^2,$$

$$\varepsilon_1 = \frac{A + B(1 - y_1)}{[(1 - y_1)^2 + Dy_1]}, \quad \varepsilon_2 = \frac{B(Dy_1)^{\frac{1}{2}}}{[(1 - y_1)^2 + Dy_1]},$$

and ε_0 is the static dielectric constant.

The simulation of IRR spectra for different ZrO_2 phases in the "residual-ray" interval was performed according to formula (4), taking into account only the phonon subsystem and the additive contribution of active optical phonons (Table). The results of the spectrum simulation were obtained with the root mean square error $\delta < 0.3 \times 10^{-2}$.

The single-oscillator model was used for the cubic ZrO_2 phase. It is the simplest because of the high symmetry of the corresponding crystal structure. For the tetragonal and monoclinic phases, models containing five [24] and seven [18], respectively, oscillators were used. The self-consistent oscillator parameters for all models are given in Table.

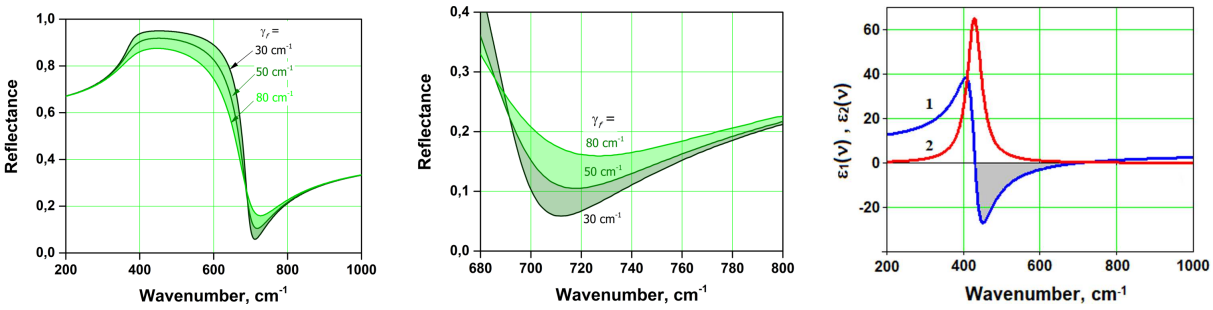

a *b* *c*

Fig. 3. Theoretical IRR spectra for the cubic ZrO_2 phase calculated for various phonon damping coefficients γ_f = 30, 50, and 80 cm^{-1} (*a*). Changes in the spectral position of the reflectance minimum in the interval 680–800 cm^{-1} (*b*). Calculated frequency dependences of the real ($\varepsilon_1(\nu)$, curve *1*) and imaginary ($\varepsilon_2(\nu)$, curve *2*) parts of the dielectric permittivity for cubic ZrO_2. The region where the existence of polaritons is possible is highlighted in gray (*c*)

The IRR spectra were modeled first for the cubic phase, and then for the tetragonal and monoclinic ones (below, they are described in this order). When approximating the experimental IR spectra, the obtained TO and LO phonon parameters had a certain uncertainty due to the overlap of spectral bands, the correlation of model parameters, and the limited spectral resolution. For single-crystalline zirconium oxide, a typical error interval was about $\pm(2\div3)$ cm^{-1}, which corresponds to the generally accepted accuracy of the IR spectroscopy method in combination with spectral modeling. At the same time, for nanostructured powders and ceramics, the error can be larger due to mode broadening and amounts to $\pm(5\div8)$ cm^{-1}.

Self-consistent parameters for ZrO_2 with different crystal structures

Parameters	ε_0	ε_∞	ν_T, cm^{-1} (γ_f, cm^{-1})	ν_L, cm^{-1} (γ_f, cm^{-1})
ZrO_2, cubic [17]	27	4.8	375 (10)	695 (10)
ZrO_2, tetragonal [24]	25	4.8	164 (97) 339 (69) 467 (106) 580 (35) 672 (172)	232 (119) 354 (95) 650 (139) 581 (39) 734 (113)
ZrO_2, monoclinic [18]	16	4.8	92 (130) 330 (55) 410 (20) 480 (30) 534 (100) 570 (60) 740 (110)	104 (260) 381 (80) 423 (28) 515 (60) 556 (138) 615 (60) 760 (120)

3.2.1. Cubic ZrO_2 phase

The IRR spectra for the cubic phase ZrO_2 were calculated using the Kramers–Kronig relations. The static dielectric constant was determined on the basis of the corresponding values for TO- and LO-phonons (Table) and using the Lyddane–Sachs–Teller relationship [26]. First, the spectra were obtained for a low value of the phonon damping coefficient, γ_f = 30 cm^{-1}; then, it was varied from 30 to 80 cm^{-1} with a step $\Delta\gamma_f$ = 5 cm^{-1}.

In Fig. 3, the curves demonstrate the spectra obtained for γ_f = 30, 50, and 80 cm^{-1}. Significant changes in the spectral shape are observed throughout the whole "residual-ray" interval, with the most pronounced variations taking place in the interval ν = 580–650 cm^{-1} (Fig. 3, *a*). An analysis of these data shows that as the phonon damping increases, the reflectance $R(\nu)$ decreases substantially: at ν = 500 cm^{-1}, R_{max} decreases from 0.95 (at γ_f = 30 cm^{-1}) to 0.87 (at γ_f = 80 cm^{-1}), and R_{min} increases from 0.06 (at γ_f = 30 cm^{-1}) to 0.15 (at γ_f = 80 cm^{-1}), with the minimum shifting from $\nu_{min} \approx 712$ cm^{-1} to ≈ 727 cm^{-1} (Figs. 3, *a* and 3, *b*).

By solving the inverse problem, the frequency dependences of the real, $\varepsilon_1(\nu)$, and imaginary, $\varepsilon_2(\nu)$, parts of the dielectric permittivity were obtained (Fig. 3, *c*). These dependences are necessary for fitting the experimental spectra; see below. For a preliminary estimation of the "residual-ray" interval, the spectral interval with anomalous dispersion is considered, where $\varepsilon_1(\nu) \le -1$. For cubic ZrO_2, this interval is observed at 400–660 cm^{-1}, which is highlighted in gray in Fig. 3, *c*. It is worth noting that the fre-

quency interval of anomalous dispersion corresponds to the region where surface phonon polaritons can exist. Their existence is of interest for the creation of various optical communication devices, in particular, for the energy transmission by means of optical signals propagating through waveguides.

3.2.2. Tetragonal ZrO_2 phase

In Fig. 4, the IRR spectra calculated for the tetragonal ZrO_2 phase in a frequency interval of 200–1000 cm^{-1}, taking into account the additive and factorized contributions of oscillators to the phonon subsystem of ZrO_2 and using the parameters given in Table, are plotted. The damping coefficients of transverse and longitudinal optical phonons were varied similarly to the simulation of the cubic ZrO_2 phase: γ_f = 30–80 cm^{-1} with a step of 5 cm^{-1}, but in Fig. 4, only the curves for γ_f = 30, 50, and 80 cm^{-1} are shown, with the region between them being tinted.

One can see that as the phonon damping increases, the phonon modes broaden and their intensity decreases. As a result, the overall reflectance decreases. The most substantial changes are observed for R_{max} at ν = 500 cm^{-1}: its value decreases from 0.9 (at γ_f = 30 cm^{-1}) to 0.7 (at γ_f = = 80 cm^{-1}). In contrast, the value of R_{min} changes insignificantly, but the minimum position shifts from $\nu_{min} \approx 786$ cm^{-1} to $\nu_{min} \approx 796$ cm^{-1} (Fig. 4, *b*).

The frequency dependences obtained theoretically for the real, $\varepsilon_1(\nu)$, and imaginary, $\varepsilon_2(\nu)$, parts of the dielectric permittivity of tetragonal ZrO_2 are shown in Fig. 4, *c*, where the spectral interval corresponding to the frequencies of surface (boundary) phonon polaritons is highlighted in gray. This interval has a larger spectral width (400–660 cm^{-1}) in comparison with that determined for cubic ZrO_2 (420–640 cm^{-1}), which makes tetragonal ZrO_2 more attractive for the creation of communication devices.

3.2.3. Monoclinic ZrO_2 phase

To calculate the spectra of the monoclinic phase, the parameter values of the corresponding TO and LO phonons (see Table) were used. In Fig. 5, the model results calculated for the *m*-ZrO_2 spectra in an interval of 200–1000 cm^{-1} using the Kramers–Kronig relations are exhibited. The phonon damping coefficient was varied in the interval $\gamma_f = 30 - 80$ cm^{-1}, and, similarly to the previous cases, only the curves

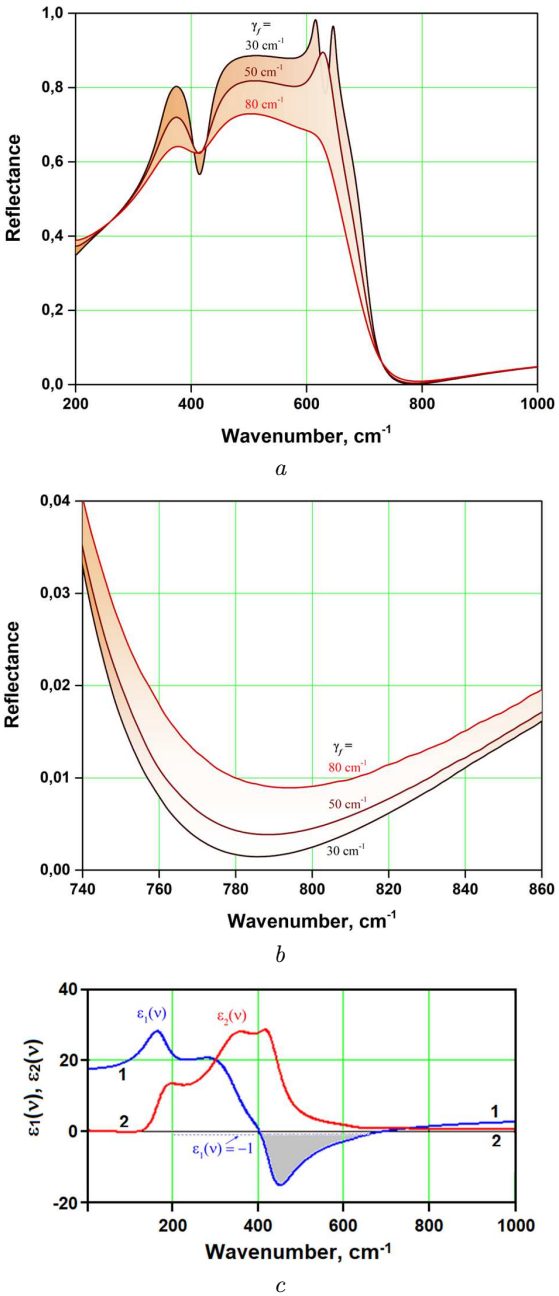

Fig. 4. Theoretical IRR spectra in the interval 200–1000 cm^{-1} for the tetragonal ZrO_2 phase calculated for various phonon damping coefficients γ_f = 30, 50, and 80 cm^{-1} (*a*). Changes in the spectral position of the reflectance minimum in a spectral interval of 740–860 cm^{-1} (*b*). Calculated frequency dependences of the real ($\varepsilon_1(\nu)$, curve *1*) and imaginary ($\varepsilon_2(\nu)$, curve *2*) parts of the dielectric permittivity for *t*-ZrO_2. The region where the existence of polaritons is possible is highlighted in gray (*c*)

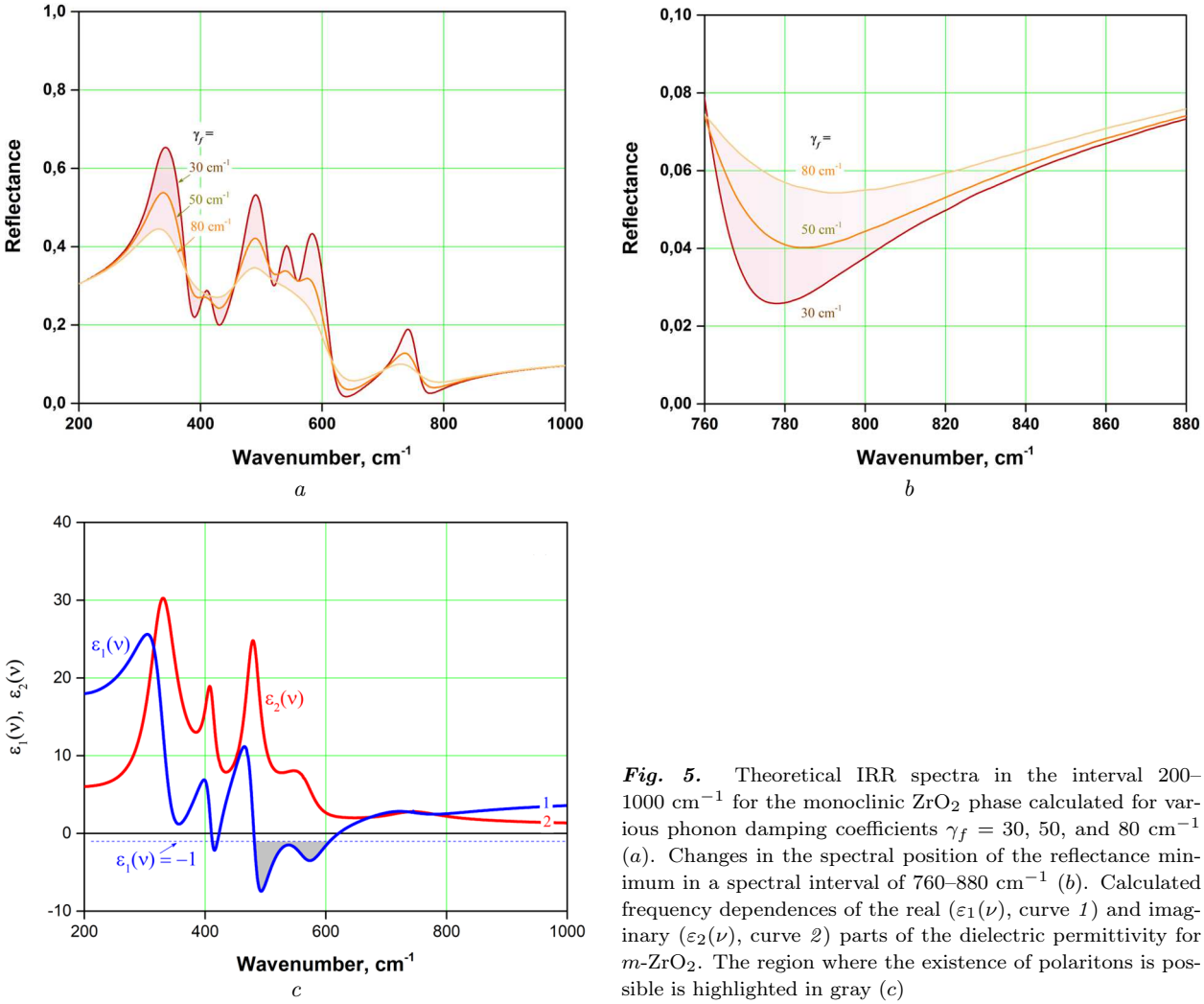

Fig. 5. Theoretical IRR spectra in the interval 200–1000 cm^{-1} for the monoclinic ZrO_2 phase calculated for various phonon damping coefficients γ_f = 30, 50, and 80 cm^{-1} (*a*). Changes in the spectral position of the reflectance minimum in a spectral interval of 760–880 cm^{-1} (*b*). Calculated frequency dependences of the real ($\varepsilon_1(\nu)$, curve *1*) and imaginary ($\varepsilon_2(\nu)$, curve *2*) parts of the dielectric permittivity for *m*-ZrO_2. The region where the existence of polaritons is possible is highlighted in gray (*c*)

for γ_f = 30, 50, and 80 cm^{-1} are shown. One can see that the growth of γ_f leads to a broadening of the phonon modes and a decrease in their intensity. As a result, the total reflectance decreases. The most noticeable changes are observed at ν = 330 cm^{-1}, where R_{max} decreases from 0.65 (at γ_f = 30 cm^{-1}) to 0.45 (at γ_f = 80 cm^{-1}). The amplitude of the high-frequency minimum increases from R_{min} = 0.027 (at γ_f = 30 cm^{-1}) to 0.055 (at γ_f = 80 cm^{-1}), which is accompanied by a shift of the minimum position to higher wavenumbers: from $\nu_{min} \approx$ 778 cm^{-1} to $\nu_{min} \approx$ 792 cm^{-1} (Fig. 5, *b*).

The obtained spectral dependences for the real, $\varepsilon_1(\nu)$, and imaginary, $\varepsilon_2(\nu)$, parts of the dielectric permittivity of ZrO_2 with a monoclinic structure are shown in Fig. 5, *c*. Unlike the cubic and tetragonal phases, the monoclinic phase exhibits two frequency "windows", where surface phonon polaritons can exist, namely, in the intervals ν = 410–420 and 480–610 cm^{-1}.

A comparison of the IR reflectance spectra calculated for different ZrO_2 phases shows that the frequency "windows" of anomalous dispersion, where $\varepsilon_1(\nu) \leq -1$, depend considerably on the structural modification of ZrO_2. They are observed in an interval of 430–656 cm^{-1} for the cubic phase, 465–652 cm^{-1} for the tetragonal phase, and in two intervals (408–423 and 482–611 cm^{-1}) for the monoclinic phase. The tetragonal modification has the widest frequency "window" of anomalous dispersion.

3.2.4. Simulation of IRR spectra taking various phonon damping coefficients into account

It should be noted that the above calculations were performed under the condition of equal damping coefficients for all phonon modes. In a real crystal structure, each phonon mode corresponds to a certain type of atomic vibrations in the lattice, and its damping coefficient is determined by the nature of those atoms (native or impurity) and can be affected by defects located nearby.

As an example, the IRR spectra of ZrO_2 with monoclinic and tetragonal structures were calculated using individual damping coefficients for each mode (see Table). The results are presented in Fig. 6, from which it follows that the IRR amplitude for the monoclinic phase is lower, and the spectral position of the minimum in the high-frequency region is shifted towards higher wavenumbers (Fig. 6, *a*) in comparison with the corresponding minimum for the tetragonal phase (Fig. 6, *b*).

3.3. Approximation and analysis of experimental IRR spectra for specimens with different crystal structures

The models described above were used to approximate the experimental spectra obtained for powders and ceramics based on zirconium oxide. Main attention was paid to their crystal structure, irrespective of the preparation conditions and the origin of impurities.

3.3.1. Specimens with a cubic structure

To analyze the IRR spectra for the cubic phase, specimens prepared on the basis of the commercial powder 10Sc1CeSZ were selected. In Fig. 7, *a*, the symbols denote experimental IRR data obtained in a spectral interval of 300–900 cm^{-1}, which corresponds to the interval shown in Fig. 2, *b* for the cubic phase. The figure also illustrates the corresponding approximation made according to the approach described above. It can be seen that the experimental curve is well described by the theoretical curve calculated taking into account only the phonons in the cubic structure (Fig. 7, *a*), which is confirmed by the Raman data. The parameters quoted in Table and the mathematical expressions (3) and (4) [26] adequately describe the spectra of cubic ceramics. The best agreement between theory and experiment was achieved for $\gamma_f = 45$ cm^{-1}, with the root mean square error $\delta = 0.3 \times 10^{-2}$.

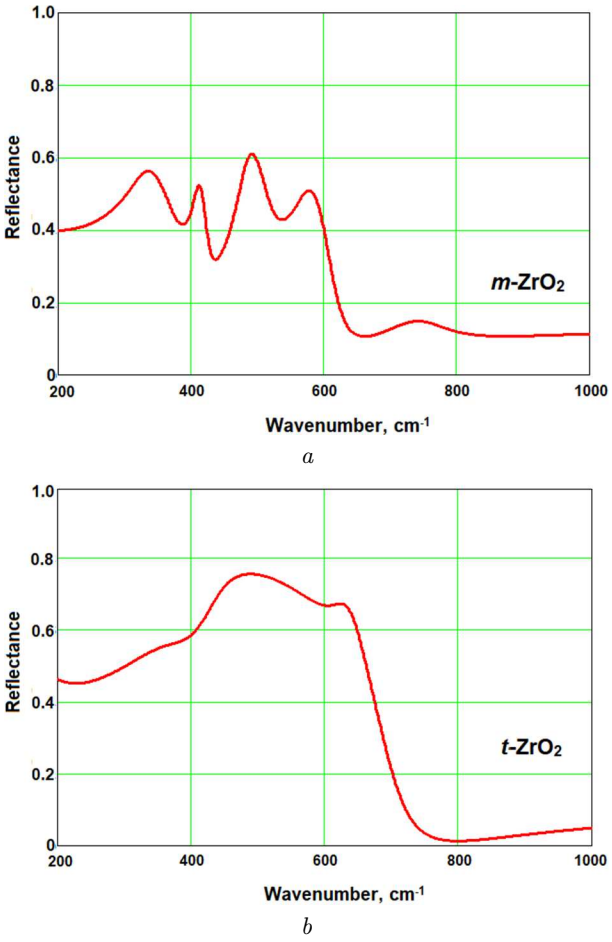

Fig. 6. IRR spectra simulated for the monoclinic (*a*) and tetragonal (*b*) ZrO_2 phases using the corresponding literature data for TO and LO phonon frequencies and damping coefficients, see Refs. [18, 24]

In Fig. 7, *b*, the experimental spectra obtained for the real and imaginary parts of the dielectric permittivity of cubic ceramics 10Sc1CeSZ in the corresponding frequency interval using the IRTracer-100 software are exhibited. Similar to the theoretical spectrum, the values $\varepsilon_1(\nu) \leq -1$ were observed in an interval of 430–656 cm^{-1}, which satisfies one of the conditions for the existence of surface phonon polaritons at the ceramic–air interface [26].

Obviously, more accurate data can be obtained by constructing the so-called reflectance surface $R(\nu, \gamma_f)$, which is a three-dimensional representation of the dependence of the reflectance R on the IR radiation frequency ν and the phonon damping coefficient γ_f. In Fig. 7, *c*, such a calculated IR re-

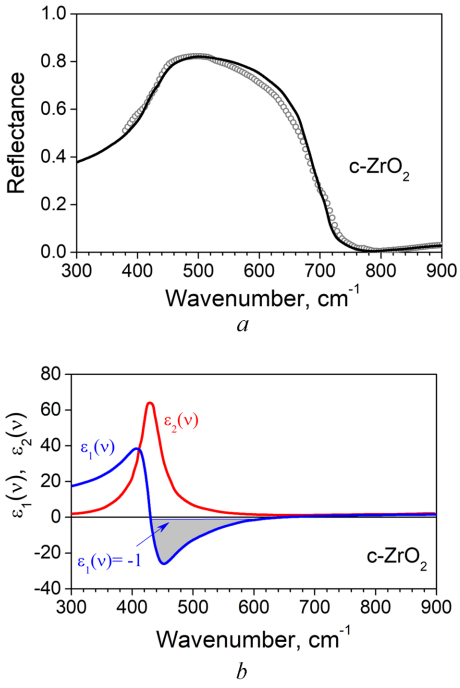

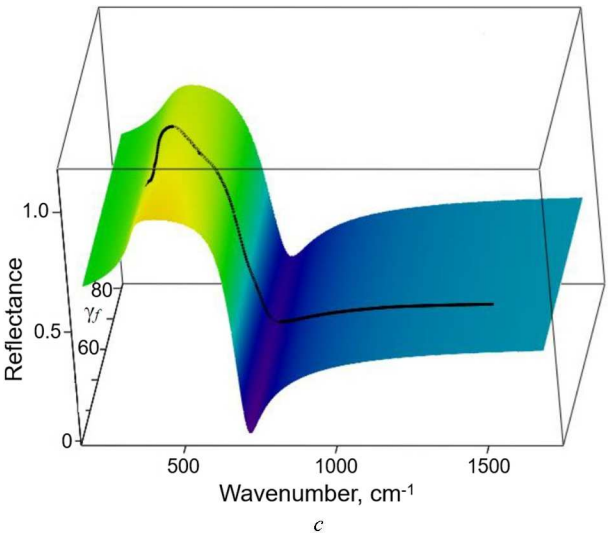

Fig. 7. Experimental spectrum (symbols) and its approximation (solid curve) for 10Sc1CeSZ ceramics; $\gamma_f = 45$ cm^{-1} (*a*). Real, $\varepsilon_1(\nu)$, and imaginary, $\varepsilon_2(\nu)$, parts of the dielectric permittivity for 10Sc1CeSZ ceramics (*b*). Calculated IRR reflectance surface and experimental spectrum for the 10Sc1CeSZ specimen (*c*)

flectance surface and experimental spectrum for the 10Sc1CeSZ sample (for comparison) are shown. The reflectance surface was calculated by scanning the phonon frequency with a step of $\Delta\nu = 1$ cm^{-1}and the phonon damping coefficient with a step of $0.01\gamma_f$. In the absence of radiation interaction with the ceramic surface, $R(\nu, \gamma_f) = 1$, and the surface is flat in this region. If phonon vibrations are excited, there appear "gaps" on the surface (Fig. 7, *c*). The depth of those "gaps" depends on the system parameters, including the IR radiation frequencies, the phonon frequencies, and the high-frequency and static dielectric constants. Calculations showed that the variation of the damping coefficient γ_f from 30 to 80 cm^{-1} has practically no effect on the spectra $R(\nu, \gamma_f)$ in the intervals of 100–360 and 800–1500 cm^{-1}. At the same time, changes in the phonon frequencies and the high-frequency and static dielectric constants lead to a substantial deformation of the spectra $R(\nu, \gamma_f)$ in the "residual-ray" region of ZrO_2 ceramics.

3.3.2. Analysis of IRR spectra for tetragonal 3YSZ ceramics

In Fig. 8, *a*, the experimental spectrum for tetragonal 3YSZ ceramics is shown (by symbols) together with the fitting curve. The calculation of $R(\nu)$ was carried out in a frequency interval of 100–1000 cm^{-1} using the parameters of the phonon subsystem quoted in Table for the tetragonal modification. The damping coefficient for the transverse and longitudinal optical phonons was determined from the Raman spectrum width. As one can see, the experimental curve agrees quite well with the calculated one for the tetragonal structure.

In Fig. 8, *b*, the experimental spectra of the real, $\varepsilon_1(\nu)$ (curve *1*), and imaginary, $\varepsilon_2(\nu)$ (curve *2*), parts of the dielectric permittivity for this ceramic are shown. The shaded area demonstrates a frequency interval of 465–652 cm^{-1}, where $\varepsilon_1(\nu) \leq -1$, so that one of the conditions for the existence of surface phonon polaritons at the *t*-ZrO_2 ceramics–air interface is fulfilled.

3.3.3. Analysis of IRR spectra for monoclinic ZrO_2 ceramics

In Fig. 9, *a*, the experimental spectrum of a specimen of monoclinic ZrO_2 ceramics (symbols) and the fitting curve are shown. The method of dispersion analysis of IRR spectra was applied to fit the frequency values of the transverse and longitudinal optical phonons of each oscillator and determine the phonon damping coefficients. The spectrum is well modeled under the

assumption that the specimen has a monoclinic structure, which is consistent with the Raman data. The frequencies of the maxima for the experimental and simulated (in parentheses) curves are 352 (357), 419 (422), 497 (497), 579 (586), and 744 cm^{-1}, which is consistent with the data of Refs. [19, 28] for this phase.

In Fig. 9, *b*, the frequency dependences of the real, $\varepsilon_1(\nu)$, and imaginary, $\varepsilon_2(\nu)$, parts of the dielectric permittivity of ZrO_2 are shown. In frequency intervals of 408–423 and 482–510 cm^{-1}, $\varepsilon_1(\nu) \leq -1$, i.e., one of the conditions for the existence of surface phonon polaritons at the *m*-ZrO_2 ceramics–air interface is also fulfilled.

3.3.4. Generalization of results

The calculation of the IRR spectra for three ZrO_2 phases showed that their minima are located in the vicinity of 700–720 cm^{-1} for *c*-ZrO_2, 790–800 cm^{-1} for *t*-ZrO_2, and 820–840 cm^{-1} for the *m*-ZrO_2 phase. The variation of the phonon damping coefficient γ_f practically does not affect the spectral position of the minimum for each phase. Thus, this feature of IR reflectance can be used to determine the crystal structure type of powders and ceramics.

The reliability of the obtained results is confirmed by the agreement of the experimental spectra registered for ceramic specimens 10Sc1CeSZ, 3YSZ, and ZrO_2, which are in the cubic, tetragonal, and monoclinic phases, respectively, with the corresponding theoretical curves. It should be noted that when considering the indicated phases, the experimentally determined characteristics of phonons were taken into account. In so doing, for undoped ZrO_2 with a monoclinic structure, phonon parameters were determined only for Zr–O bonds. At the same time, in stabilized ZrO_2, which has a tetragonal or cubic structure, the Zr–O phonon modes have already been affected by the presence of impurity atoms (Y^{3+}, Sc^{3+}, and Ce^{3+}/Ce^{4+}). In this case, it is possible to evaluate the shift of these modes with respect to the Zr–O bonds.

Indeed, doping zirconium oxide with Y^{3+}, Sc^{3+}, and Ce^{3+}/Ce^{4+} ions significantly affects not only the phase stability of the material but also the crystal lattice dynamics and phonon characteristics. It is known that the substitution of Zr^{4+} ions (an ionic radius of ≈0.84 Å for the coordination number $CN = 8$) by cations with different charges and sizes – namely,

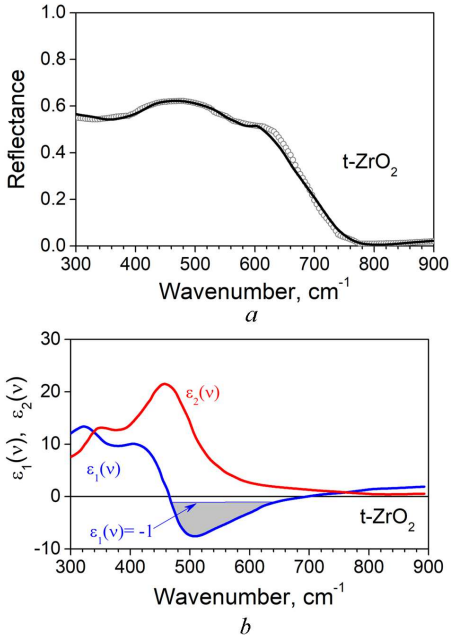

Fig. 8. Experimental spectrum (symbols) and its approximation (solid curve) for tetragonal 3YSZ ceramics; $\gamma_f = 45$ cm^{-1} (*a*). Real, $\varepsilon_1(\nu)$, and imaginary, $\varepsilon_2(\nu)$, parts of the dielectric permittivity for 3YSZ ceramics (*b*)

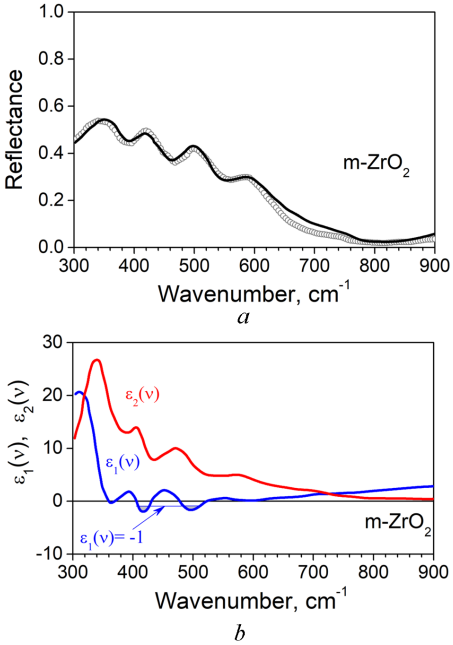

Fig. 9. Experimental spectrum (symbols) and its approximation (solid curve) for monoclinic ZrO_2 ceramics (*a*). Real, $\varepsilon_1(\nu)$, and imaginary, $\varepsilon_2(\nu)$, parts of the dielectric permittivity for ZrO_2 ceramics (*b*)

Y^{3+} (≈1.02 Å), Sc^{3+} (≈0.87 Å), and Ce^{3+}/Ce^{4+} (≈1.14 Å/≈0.97 Å) – brings about local lattice distortions and the formation of oxygen vacancies necessary for charge compensation. Such defect states change the local force constants of Zr–O bonds and govern the evolution of the phonon characteristics of stabilized ZrO_2 depending on the impurity type and concentration.

The presence of impurity atoms reduces the effective stiffness of the crystal lattice, which manifests itself in a partial "softening" of phonon modes. At the same time, the expected frequency shifts, as a rule, have a moderate magnitude and usually do not exceed several wavenumbers. A typical shift is about 2–8 cm^{-1} for systems doped with yttrium and 1–4 cm^{-1} for Sc-stabilized ZrO_2, whereas in the case of doping with cerium, shifts of up to 10 cm^{-1} are possible due to the significantly larger cerium mass, and such shifts are often combined with an asymmetric broadening of the spectral bands. More substantial frequency changes are associated, as a rule, with phase transformations rather than the direct influence of impurity atoms (when their concentration is low).

The phonon modes most sensitive to doping are low-frequency modes with frequencies below 300–350 cm^{-1}, which correspond to collective translational and angular (rotational) vibrations of Zr–O polyhedra. It is these modes that respond to local lattice distortions and the presence of oxygen vacancies and demonstrate a noticeable, although small, shift of their maxima. For vibrations of Zr–O bonds in the mid-IR interval (400–650 cm^{-1}), changes in the spectral positions of the maxima are usually less pronounced, and, as evidenced by the increase of the phonon damping coefficients, the broadening of the spectral bands becomes the dominant effect.

From the experimental viewpoint, small shifts of phonon modes can be reliably registered using the Raman method (provided that the spectral resolution of the corresponding spectral instruments is sufficient). In the IRR spectra, where the band widths are significant, the influence of impurities is usually observed as mainly a change in the shape and intensity of vibrational bands, rather than a distinct shift of their maxima. Thus, the main spectral manifestation of ZrO_2 doping is less a shift of phonon frequencies than an increase in the damping coefficients due to enhanced phonon scattering at point defects, oxygen vacancies, and local elastic stress fields.

It is also necessary to take into consideration the limitations of phase identification in the case of materials with a mixed crystal structure. Different ZrO_2 phases are characterized by phonon modes that are close in position: the difference between them often does not exceed a few wavenumbers. In the presence of a substantial band broadening induced by impurities, oxygen vacancies, or the nanoscale nature of the investigated materials, the contributions of individual phases can partially overlap. Under such conditions, the IRR spectroscopy is an effective tool for detecting general structural changes and phase transformation trends. A comparison of the IRR spectra of the monoclinic, tetragonal, and orthorhombic phases of ZrO_2 testifies that the phonon mode at 740–760 cm^{-1} is inherent only to the monoclinic phase, whereas other phonon modes have similar spectral characteristics. Therefore, an appreciable contribution of this band to the IRR spectrum makes it possible to state the presence of the monoclinic phase in the examined specimen, whereas the absence of this mode means the absence of this phase or its insignificant contribution. At the same time, a quantitative determination of phases with close concentrations requires a combination with other methods of structural analysis. The creation of a method for determining the phase ratio by combining the Raman, IRR, X-ray diffraction, and electron microscopy is a direction of further research.

4. Conclusions

To summarize, external IRR spectra were calculated on the basis of a developed mathematical model that takes into account the additive (the cubic modifications) and phenomenological (the monoclinic and tetragonal modifications) contributions of oscillators to the dielectric function. It was shown that the calculated IRR spectra are in good agreement with the experimental data presented both in this work and in the works of other authors. A family of calculated IRR curves for c-ZrO_2 was obtained for various phonon damping coefficients and IR radiation frequencies.

It was shown that changes in the damping of the phonon subsystem substantially affect the reflectance spectrum in the interval of the "residual-ray" maximum. It was found that ZrO_2 ceramics can be well modeled following the method described for zirconium oxide single crystals with the $E \perp c$ orienta-

tion and using mutually consistent parameters obtained by the Raman method. This fact confirms the prospects of the non-destructive IR spectroscopy method in determining the optical characteristics of not only single crystals, but also polycrystalline samples (powders, thick layers, and ceramics).

The complex combination of IRR and Raman methods provides the possibility of rapid structural characterization of ZrO_2-based materials. It can be used to determine the transformation of the crystal structure both during doping and as a result of various heat treatments.

1. N. Korsunska, L. Khomenkova. Multifunctional Zirconia-based Nanocomposites. In *Solid State Composites and Hybrid Systems*. Edited by R. Savkina, L. Khomenkova (CRC Press, 2018), p .28.
2. I.O. Polishko, Y.M. Brodnikovskyi, D.M. Brodnikovskyi, N.O. Lysunenko, O.M. Myslyvchenko, O.V. Dudnik, M.Yu. Smirnova-Zamkova, I.O. Marek, A.V. Kotko, O.D. Vasylyev, L.Yu. Khomenkova, R.V. Horda, L.L. Kovalenko, N.O. Korsunska, A.G. Bilous. ZrO_2-based nanopowders for fuel cells and catalysis. In: *2022 IEEE 12th International Conference Nanomaterials: Applications & Properties (NAP), Krakow, Poland, 2022* (IEEE NAP-2022), p. 1.
3. E.F. López, V.S. Escribano, M. Panizza, M.M. Carnasciali, G. Busca. Vibrational and electronic spectroscopic properties of zirconia powders. *J. Mater. Chem.* **11**, 1891 (2001).
4. S.N. Basahel, T.T. Ali, M. Mokhtar, K. Narasimharao. Influence of crystal structure of nanosized ZrO_2 on photocatalytic degradation of methyl orange. *Nanoscale Res. Lett.* **10**, 73 (2015).
5. N. Korsunska, M. Baran, A. Zhuk, Y. Polishchuk, T. Stara, V. Kladko, Y. Bacherikov, Y. Venger, T. Konstantinova, L. Khomenkova. Role of paramagnetic defects in light emission processes in Y-doped ZrO_2 nanopowders. *Mater. Res. Expr.* **1**, 045011 (2014).
6. M. Asadikiya, Y. Zhong. Oxygen ion mobility and conductivity prediction in cubic yttria-stabilized zirconia single crystals. *J. Mater. Sci.* **53**, 1699 (2017).
7. Y. Wang, Z. Zhu, S. Ta, Z. Cheng, P. Zhang, N. Zeng, B.A. Goodman, S. Xu, W. Deng. Optical properties of yttria-stabilized zirconia single-crystals doped with terbium oxide. *Crystals* **12**, 1081 (2022).
8. D. Gazzoli, G. Mattei, and M. Valigi. Raman and X-ray investigations of the incorporation of Ca^{2+} and Cd^{2+} in the ZrO_2 structure. *J. Raman Spectrosc.* **38**, 824 (2007).
9. Q. Xue, X. Huang, L. Wang, J. Dong, H. Xu, J. Zhang. Effects of Sc doping on phase stability of $Zr_{1-x}Sc_xO_2$ and phase transition mechanism: First-principles calculations and Rietveld refinement. *Mater. Design* **114**, 297 (2016).
10. K. Smits, D. Olsteins, A. Zolotarjovs, K. Laganovska, D. Millers, R. Ignatans, J. Grabis. Doped zirconia phase and luminescence dependence on the nature of charge compensation. *Sci. Rep.* **7**, 44453 (2017).
11. K. Park, S.J. Yoon, J.W. Pi. Tunable photoluminescence properties of nano-sized $Zr_{1-x}O_2 : xDy^{3+}$ phosphors. *Dyes Pigm.* **143**, 317 (2017).
12. S.K. Tadokoro, E.N.S. Muccillo. Synthesis and characterization of nanosized powders of yttria-doped zirconia. *J. Alloys Compound.* **344**, 186 (2002).
13. K. Smits, A. Sarakovskis, L. Grigorjeva, D. Millers, J. Grabis. The role of Nb in intensity increase of Er ion upconversion luminescence in zirconia. *J. Appl. Phys.* **115**, 213520 (2014).
14. O. Marie, X. Portier, N. Korsunska, L. Khomenkova. CO–PROX reactions on copper Y_2O_3–ZrO_2 catalysts prepared by a single step co-precipitation technique. *Appl. Catal. B* **278**, 119258 (2020).
15. L. Khomenkova, O. Marchylo, Y. Polishchuk, S. Ponomaryov, O. Isaieva, I. Vorona, L. Melnichuk, X. Portier, O. Melnichuk, N. Korsunska. Effect of dopant loading and calcination conditions on structural and optical properties of ZrO_2 nanopowders doped with copper and yttrium. *Mater. Res. Exp.* **11**, 065005 (2024).
16. M.A. Waghmare, K.S. Pawar, H.M. Pathan, A.U. Ubale, Influence of annealing temperature on the structural and optical properties of nanocrystalline zirconium oxide *Mater. Sci. Semicond. Process.* **72**, 122 (2017).
17. A. Feinberg, C.H. Perry. Structural disorder and phase transitions in ZrO_2–Y_2O_3 system. *J. Phys. Chem. Sol.* **42**, 513 (1981).
18. C.H. Perry, F. Lu, D.W. Liu, B. Alzyab. Phonons and phase transitions in zirconia. *J. Raman Spectrosc.* **21**, 577 (1990).
19. C.M. Phillippi, K.S. Mazdiyasni. Infrared and Raman spectra of zirconia polymorphs. *J. Am. Ceram. Soc.* **54**, 254 (1971).
20. N. Korsunska, M. Baran, I. Vorona, V. Nosenko, S. Lavoryk, Y. Polishchuk, V. Kladko, X. Portier, L. Khomenkova. Effect of cooling rate on dopant spatial localization and phase transformation in Cu-doped Y-stabilized ZrO_2 nanopowders. *Phys. Status Solidi C* **14**, 1700183 (2017).
21. L. Khomenkova, D. Lehninger, O. Kondratenko, S. Ponomaryov, O. Gudymenko, Z. Tsybrii, V. Yukhymchuk, V. Kladko, J. Von Borany, J. Heitmann. Effect of Ge content on the formation of Ge nanoclusters in Magnetron-Sputtered $GeZrO_x$-based structures. *Nanosc. Res. Lett.* **12**, 196 (2017).
22. D. Khomenkov, D. Lehninger, L.Yu. Melnichuk, J. Heitmann, O.V. Melnichuk. Spectroscopic characterization of thermostimulated transformation of thin films based on transition metal oxides doped with germanium. *J. Nano Electron. Phys.* **17**, 06033 (2025).
23. N. Korsunska, M. Baran, I. Vorona, V. Nosenko, S. Lavoryk, X. Portier, L. Khomenkova. Impurity governed modification of optical and structural properties of ZrO_2-based composites doped with Cu and Y. *Nanosc. Res. Lett.* **12**, 157 (2017).

24. C. Pecharromán, M. Ocaña, C.J. Serna. Optical constants of tetragonal and cubic zirconias in the infrared. *J.Appl. Phys.* **80**, 3479 (1996).
25. I.V. Venger, E.F. Venger, L.Yu. Melnychuk, O.V. Melnychuk. *Anisotropy of Surface Plasmon-Phonon Polaritons in ZnO and 6H–SiC Single Crystals* (Naukova Dumka, 2020) (in Ukrainian).
26. O. Melnichuk, L. Melnichuk, E. Venger. Phonon and plasmon-phonon interactions in ZnO single crystals and thin films. In: *Oxide-Based Materials and Structures*. Edited by R. Savkina, L. Khomenkova (CRC Press, 2020), p. 163.
27. O.V. Melnichuk, N.O. Korsunska, I.V. Markevich, V.V. Boyko, Yu.O. Polishchuk, Z.F. Tsybrii, L.Yu. Melnichuk, Ye.F. Venger, V.P. Kladko, L.Yu. Khomenkova. Peculiarities of specular infrared reflection spectra of ZnO-based ceramics. *Semicond. Phys. Quant. Electron. Optoelectron.* **24**, 390 (2021).
28. M. Sternik, K. Parlinski. Lattice vibrations in cubic, tetragonal, and monoclinic phases of ZrO_2. *J. Chem. Phys.* **122**, 064707 (2005).

Received 24.11.25.
Translated from Ukrainian by O.I. Voitenko

Д.В. Хоменков,
Л.Ю. Мельничук, О.В. Мельничук

ОСОБЛИВОСТІ СПЕКТРІВ
ІНФРАЧЕРВОНОГО ВІДБИВАННЯ
МАТЕРІАЛІВ НА ОСНОВІ ZrO_2
З РІЗНОЮ КРИСТАЛІЧНОЮ БУДОВОЮ

У цій роботі продемонстровано застосування спектроскопії інфрачервоного відбивання для ідентифікації кристалічних фаз у матеріалах на основі ZrO_2. Наведено експериментальні спектри порошків та кераміки з різною будовою, а також запропоновано теоретичні моделі для апроксимації спектрів ІЧ-відбивання на основі частотної залежності діелектричної проникності, описаної формулою Гельмгольца–Кеттлера. Розрахунки виконувалися із застосуванням співвідношень Крамерса–Кроніга. Для опису кубічної, тетрагональної та моноклінної фаз ZrO_2 використовувалися моделі з одним, п'ятьма й сімома осциляторами, відповідно. Проведено моделювання з урахуванням коефіцієнтів затухання фононів. Отримані результати показали наявність вираженого мінімуму відбивання у високочастотній області спектра. Його спектральне положення відповідає високочастотній межі смуги "залишкових променів", яка є специфічною для різних фаз. Цей мінімум з'являється в діапазонах 710–720 $см^{-1}$ для кубічного ZrO_2, 790–800 $см^{-1}$ для тетрагонального ZrO_2 і 820–840 $см^{-1}$ для моноклінного ZrO_2. Показано, що коефіцієнти затухання фононів впливають на форму спектра ІЧ-відбивання, але чинять лише незначний вплив на спектральне положення високочастотного мінімуму. Цей фактор разом з аналізом форми спектра може бути надійним спектральним маркером для ідентифікації кристалічних фаз. Аналіз експериментальних спектрів дав змогу оцінити статичну й високочастотну діелектричні проникності, частоти поперечних і поздовжніх оптичних фононів та відповідні коефіцієнти затухання для порошків і кераміки з різною кристалічною будовою на основі ZrO_2.

Ключові слова: ZrO_2, кристалічна структура, коливальні спектри, інфрачервона спектроскопія відбивання, моделювання.